

MASS under strong scintillation

A. Tokovinin

Version 1. October 22, 2004

1 Introduction

The MASS instrument measures scintillation indices (normal and differential) in 4 concentric apertures A,B,C,D. The data are fitted to a model of 6 layers at fixed altitudes that represents the measured indices by linear combinations of the layer intensities (i.e. turbulence integrals in $m^{1/3}$) with weighting functions (WFs). The WFs are computed using the standard weak-perturbation theory applicable in the regime of weak scintillation. This theory was extended from the standard monochromatic case to treat correctly scintillation in a wide spectral band.

As a justification of the linear theory, Roddier (1981, p.329) writes that “Saturation regimes usually occur when the distance from zenith exceeds 60° . Near the zenith, they are exceptional...”. In practice the scintillation index measured by MASS in the 2-cm aperture A exceeds 0.2 quite frequently. The index is a *square* of relative intensity fluctuations, so 0.2 means that the light intensity in the pupil fluctuates by a factor of 2, making the non-linear effects quite significant. Indices exceeding one have been measured occasionally. It has been found that MASS over-estimates the seeing in these conditions. Its capacity of turbulence profile (TP) restoration also becomes questionable, as it critically depends on the WFs.

Here we simulate light propagation in the atmosphere numerically and compare the results with the weak-perturbation theory. The implications for the interpretation of the MASS results are discussed.

2 Simulation tools

2.1 Atmospheric simulator: `simatm.pro`

Simulation of turbulence is widely used nowadays, e.g. in adaptive optics. As a starting step, we took the “Turbulenz” code in IDL from Heidelberg (<http://www.mpia-hd.mpg.de/AO/ATMOSPHERE/TurbuLenZ/tlz.html>). Given the Fried parameter r_0 for a layer, the code outputs a phase screen generated by spectral technique: the Fourier Transform (FT) of the phase is generated as an array of zero-mean Gaussian random numbers, their amplitudes increasing at low frequencies f as $f^{-11/6}$. The underlying phase power spectrum W_ϕ (in square meters) is

$$W_\phi = 0.023 f^{-11/3} r_0^{-5/3}. \quad (1)$$

It is well known that this method underestimates the low-frequency part of turbulence, and, notably, produces wrong phase structure functions. The reason is that any function obtained by discrete FT is periodic, with a period equal to the grid size. Thus, the structure function initially increases, reaches a maximum at half-grid-size and then gracefully drops to zero again at a separation

equal to the grid size. Additional steps are usually taken to overcome this (like adding sub-harmonics), but then the simulated phase is no longer periodic. We are interested here in the scintillation which effectively filters only high spatial frequencies. So, no sub-harmonics were added.

The propagation of wave-fronts is simulated by the spectral technique, again using the FT. A code in C for light propagation was written by Gleb Vdovin and can be found at <http://www.okotech.com/>. Briefly, if $U_1(\vec{r})$ is the amplitude of the light waves before propagation, and $A_1(\vec{f})$ is its FT, then the FT of amplitude after propagation is obtained by frequency filtering:

$$A_2(\vec{f}) = A_1(\vec{f}) \exp(-i\pi z \lambda f^2), \quad (2)$$

where z is the propagation distance, $f = |\vec{f}|$.

This method is computationally fast, involving only two FFTs. Its drawback, however, is that in fact it simulates propagation in a rectangular waveguide of grid size with reflective walls. In order to approximate propagation in the free space, numerical “absorption” is sometimes added near the “walls”. Alternatively, beam size must be some 2 times smaller than the grid size, so that the intensity near the walls is negligible. However, propagation of periodic phase screens does not present problems near the grid boundaries because amplitude continues smoothly outside the boundaries. This is why in our simulations periodic phase screens can be propagated any distance without artifacts near grid boundaries.

The code `simatm.pro` presently simulates two turbulent layers. Its input parameters are the half-size of the computational grid in pixel (512 recommended, but 256 works faster), the physical size of the pixel (5mm or 2.5mm), the wavelength (we used 0.45 μm , close to the MASS effective wavelength), the total seeing, the fraction of turbulence in the high layer, and the altitudes of the two layers. If the fraction is zero, only the low layer is simulated and the additional propagation step is skipped. This makes things faster and closer to 1-layer theory. The calculations are done in double precision (otherwise the intensity distribution is wrong). The output is saved in `atm.idl` as 2-dimensional complex amplitude, accompanied by the input parameters.

The limitation of the above simulation is monochromatic light (we know that finite bandwidth does modify the WFs) and the displacement of all layers with the same speed (in the real atmosphere the layers move with different speeds). The number of simulated layers can be increased easily, but two are sufficient for this study.

2.2 MASS simulator: `simmass2.pro`

The code `simmass2.pro` simulates the temporal and spatial variation of the light intensity detected by the MASS apertures. The complex amplitude screen is converted to the light intensity with average value of one. A suitable portion of n_{csr}^2 size is cut out from this large screen and integrated over the MASS ring apertures. At each subsequent exposure, the selected portion is shifted by $j_{step} = V * T / p$ pixels (V is the wind speed, T is the exposure time, p is the pixel size of the atmospheric screen). Only integer shifts are allowed, so the “effective wind speed” is calculated after rounding. If zero wind speed is specified, the j_{step} is set to 1 pixel.

We take advantage of the periodic properties of the screens. As the selected portion approaches the right border of the array, the array is left-shifted. The screen can be visualized as a cylinder of infinite length. In order to sample the whole cylinder efficiently, we add small shifts in the y-direction, so that the apertures slide a certain length per full screen width (Fig. 1). The slide angle is small and is neglected as far as effective wind is concerned. The default slide is twice the largest aperture. As the trajectory approaches the upper limit of the array, the y-shift is performed. We arrange the

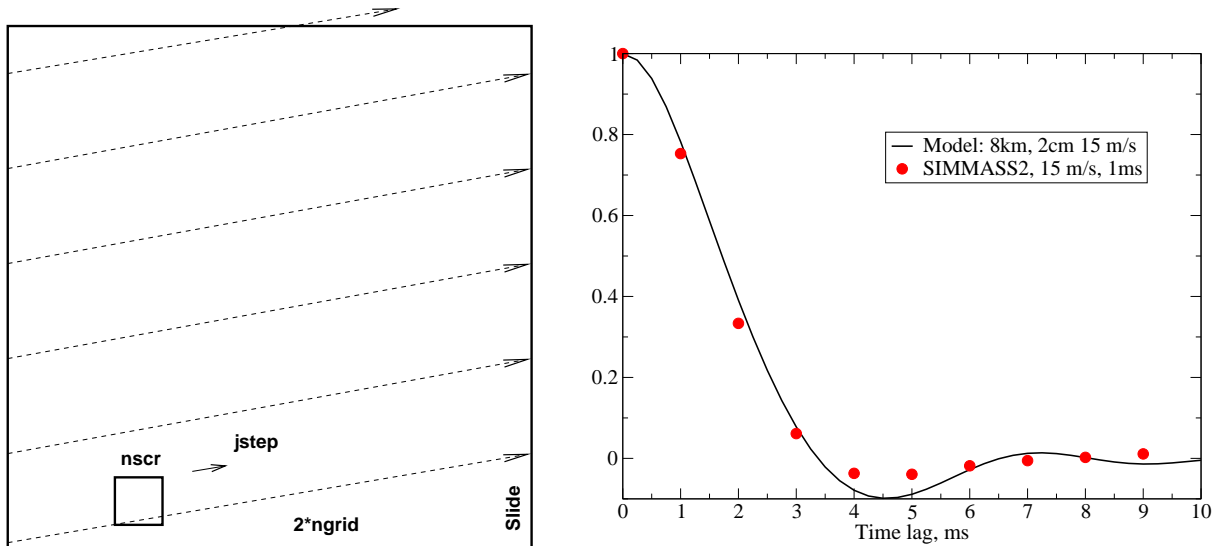


Figure 1: Left: Simulation of MASS aperture motion over the atmospheric screen.

Figure 2: Right: The simulated temporal autocorrelation function for 2-cm aperture is compared to the theoretical model.

slide to be an odd number of pixels, so that when the same part of the array is sampled again, the trajectory does not repeat exactly.

With the typical simulation parameters, the screen size is 5.12 m. The slide is 16 cm, giving 32 passes or an effective trajectory length of 163 m. With a wind velocity of 15 m/s, some 10-s exposure samples the whole screen. We usually simulated 20-s accumulation time.

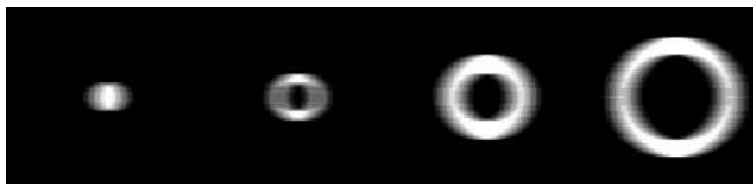


Figure 3: Four MASS ring apertures A,B,C,D “trailed” by 1.5 cm, corresponding to a shift during 1 ms exposure under 15 m/s wind.

During 1-ms MASS exposure time the intensity pattern is shifted with respect to the apertures, decreasing the measured scintillation. Instead of shifting the screen, we trail (smear) the apertures by a suitable amount (Fig. 3). The apertures are defined on a grid over-sampled by a factor of 2 or 4 with respect to the original screen. At the beginning of the calculation, the aperture transmission (1 inside, zero outside) is shifted and averaged, producing “trailed” apertures. Those are multiplied by the selected portion of the intensity screen (also over-sampled, with linear interpolation) and integrated. Thus, series of 4 intensity samples (each 20000 points for 20-s accumulation) are generated.

The intensities serve to compute the scintillation indices (normal and differential) by both linear and logarithmic formulas. Moreover, the correlation between successive intensity samples is computed in order to simulate the “zero-exposure” correction as implemented in MASS. For zero wind, there

is no aperture trailing, but the screen still shifts between exposures, so in this case the correlation is meaningless.

To test the correctness of the temporal behavior, we computed the auto-correlation function (ACF) of the simulated intensities and compared it with the theoretical ACF derived for the same model from the temporal power spectrum (program `tempsp.pro`). The results shown in Fig. 2 are quite satisfactory.

Extensive tests of `simatm.pro` and `simmass2.pro` show that under weak scintillation these tools faithfully reproduce the expected theoretical behavior. The scintillation indices match the WF-calculated ones to within 2%. The spatial spectrum of the intensity fluctuations also corresponds to theory. Thus, we are confident that the tools do not contain any major errors. We also checked that the numerical parameters (grid size, pixel size, over-sampling) can be changed by factors of at least two around their best selected values without large effect on the results.

2.3 Simulation package

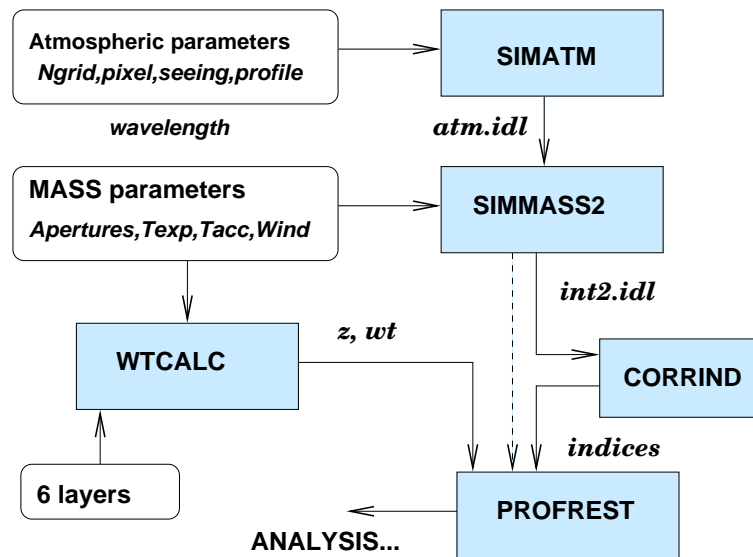


Figure 4: Relation between the components of the simulation IDL package.

The relation between various components of the simulation package is shown in Fig. 4. The two major programs are described above. The routine `wtcalc.pro` computes the theoretical WFs for a set of MASS apertures and a grid of altitudes. Our standard logarithmic grid (0.5, 1, 2, ... 16 km) was used. The procedure `profrest.pro` takes the set of 10 scintillation indices delivered by `massim2.pro` and the weights to compute the “restored” profile that can be compared to the initial 2-layer model. Thus, the effects of saturated scintillation or finite exposure time can be evaluated. An attempt to correct the saturated indices is implemented in the code `corrind.pro`, so that corrected data can replace the raw one in the restoration.

3 Results

3.1 Spatial structure of saturated scintillations

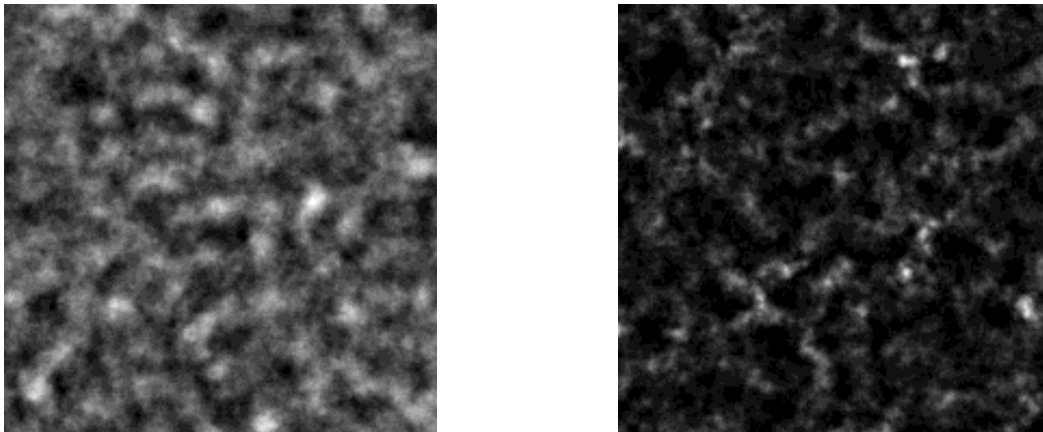


Figure 5: Intensity screens of 1 m^2 size in conditions of weak scintillation (left, $0.2''$ seeing, 1 layer at 10 km) and strong scintillation (right, $1''$ seeing, equal layers at 2 and 10 km)

The linear theory of weak scintillation presumes that each frequency component of the phase screen gives rise to the intensity fluctuations of the same spatial frequency, with its amplitude being determined by the Fresnel propagation factor. Indeed, the Fresnel propagation is a linear operator with respect to the complex amplitude of the light waves. However, it is not linear with respect to phase or amplitude. Moreover, the intensity is the square modulus of the amplitude. These non-linear operations give rise to harmonics of each frequency and to cross-talk between frequencies. Generally, we expect that as scintillations approach saturation, the high-frequency content of the intensity fluctuations would increase because the energy will be transferred from low to high spatial frequencies.

Under weak scintillations, the intensity fluctuations on the ground are distributed more or less symmetrically around the mean value. Strong scintillations are characterized by bright spikes amidst the “dark” background (Fig. 5). All things being equal, the spiky pattern contains more high frequencies. This is indeed borne out by the simulations (Fig. 6). The theoretical form of the spatial spectrum dominated by the ripples of the Fresnel term is reproduced faithfully only under very good seeing. The deviations become apparent already at $0.5''$ seeing, when the scintillation index is as low as 0.14. Under the typical seeing of $1''$ the mis-match is already well developed, becoming catastrophic under the $2''$ seeing.

MASS distinguishes individual turbulent layers by the spatial filtering of fluctuations with its ring apertures. The differential indices correspond to band-pass filters and play a crucial role in constraining the turbulence integral. As the power spills to high frequencies, the differential indices become over-estimated (thus over-estimating the seeing) and the normal indices saturate.

3.2 MASS simulation

An extensive run of MASS simulations has been done (code `run2.pro`). The extract of the code shows major parameters used in this simulation.

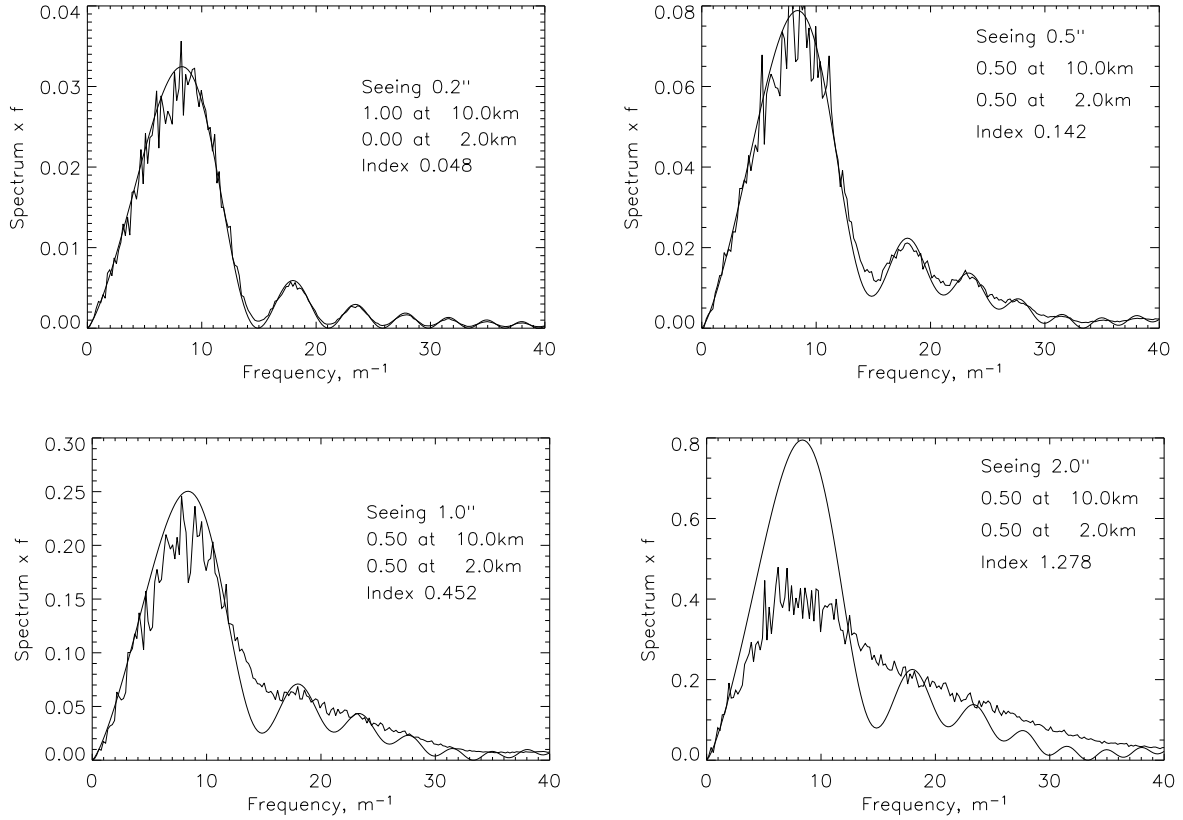


Figure 6: Radially-averaged spatial power spectra of simulated intensity fluctuations corresponding to progressively increasing scintillation. The smooth lines depict theoretical spectra. The area under the curves is directly proportional to the contribution of individual frequencies.

```

lambda = 0.45e-6 ; wavelength
ngrid = 512      ; 1024x1024 grid
pixel = 0.0025  ; 2.5mm pixels
zlow = 2000     ; low layer at 2km
zhigh = 10000   ; high layer at 10km
see = [0.3,0.6,0.9,1.2,1.5,1.8,2.1] ; seeing, arcseconds
d = [1.9,3.15,5.6,8.0]*0.01 ; aperture diameter, m: Meade
texp = 0.001    ; exposure time, s
tacc = 20       ; accumulation time, s
prof=[[1,0],[0.9,0.1],[0.5,0.5],[0,1]]

```

For each value of seeing, 4 different TPs were simulated, with the high-layer fraction of 0, 0.1, 0.5, and 1 (hereafter profiles 1 to 4, respectively). For each profile and seeing, MASS was simulated for wind speeds of 0, 10, and 20 m/s. The arrays of scintillation indices (exposure-corrected and uncorrected) are saved in `run2.id1` for further analysis.

The simulated scintillation indices are compared to the small-perturbation theory in Fig. 7. The excellent match is obtained under good seeing. As the seeing degrades, the normal indices become

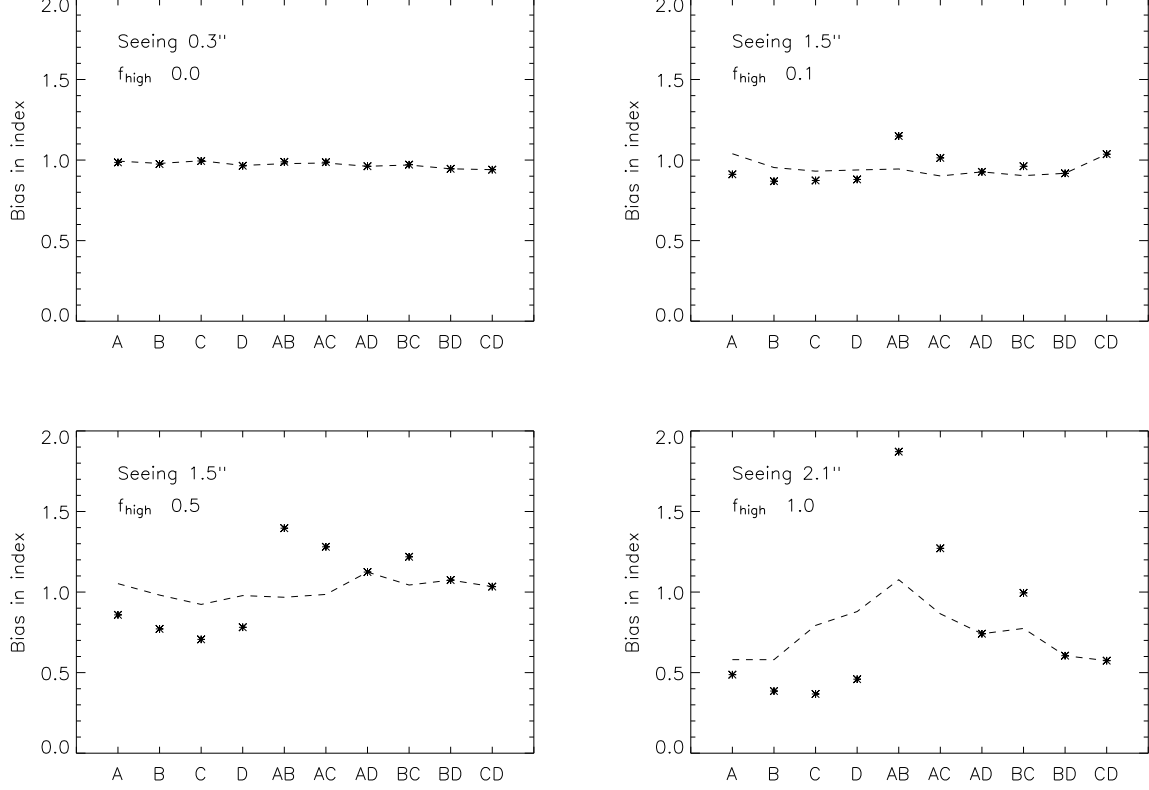


Figure 7: The ratio of the simulated scintillation indices to theoretical ones under different conditions (asterisks) and attempted corrections (dashed lines). The wind velocity is zero.

less than expected (saturate) and most differential indices become larger. This behavior is a direct consequence of the modified spatial spectrum of intensity fluctuations. The mis-match between the simulations and theory does not depend only on seeing, but rather on the amplitude of the scintillations. Thus, the same $1.5''$ seeing can have either large or small deviations of indices from theory.

3.3 Index correction

The simulation results were studied in hope to find some way to correct the measured indices for the effect of saturation. This attempt has met with only partial success because the effect depends on two parameters – seeing and TP. The formula that were coarsely fitted to the “correction vs. index” plot (Fig. 8) give the ratio f of measured and expected values for each index as a function of measured indices. Thus, we have to divide the measured indices by f . The formulas implemented in `corrind.pro` and used in Fig. 7 are:

$$f_A = 1 - 0.5A + 0.33A^2 \quad (3)$$

$$f_B = 1 - 0.5B \quad (4)$$

$$f_C = 1 - 0.5C - 2C^2 \quad (5)$$

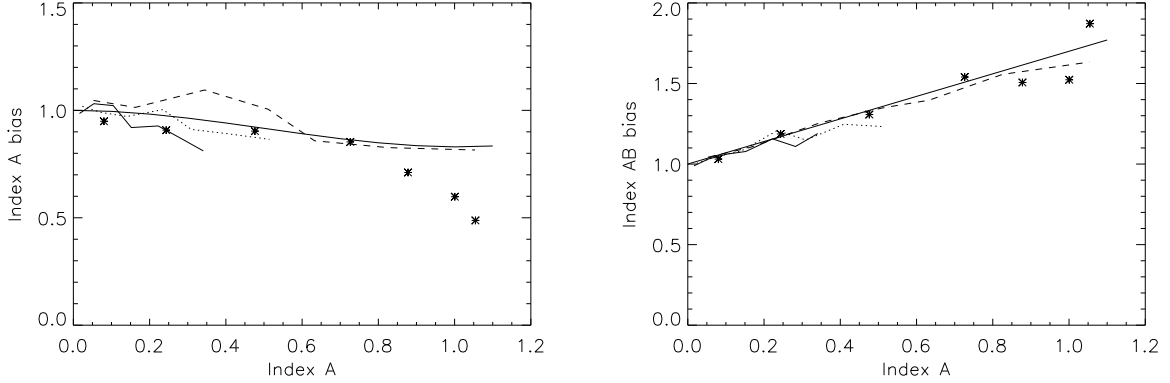


Figure 8: The dependence of simulated indices (A, left; AB, right) on the scintillation index in the aperture A. Full, dotted, dashed lines and asterisks correspond to profiles 1,2,3,4, respectively. The proposed corrections are plotted in full lines as well.

$$f_D = 1 - D - 3.3D^2 \quad (6)$$

$$f_{AB} = 1 + 0.7A \quad (7)$$

$$f_{AC} = 1 + 0.7B \quad (8)$$

$$f_{BC} = 1 + 0.7C \quad (9)$$

No correction is applied to the differential indices AD, BD and CD.

We noted that the correction for AB works rather well in all conditions (Fig. 8). This is a good news because this index is mostly used to estimate the total integral and seeing. In all cases the correction brings the indices closer to their expected values, achieving a match to 10everything fails).

3.4 Effect of saturation on profile restoration

The turbulence profiles restored from the raw and corrected indices are plotted in Figs. 9,10. As expected, under partial saturation the increased power at high frequencies translates to the downward shift of the restored profile. At the same time the seeing is over-estimated due to the bias in differential indices (“overshoots”).

The influence of saturation is partially removed with the proposed correction of indices. Limiting ourselves to moderate seeing (better than $1.8''$), we see that the localization of turbulent layers definitely improves when the correction is applied. The worst case is profile 3 when the success of the correction remains questionable.

The restoration procedure depends on the delicate balance between the measured indices, it is sensitive to the index errors at 1-2% level. Clearly, the crude correction suggested above is insufficient. It has not been tested on an more extensive set of profiles. We hope that a better way to interpret semi-saturated scintillation will result from a deeper understanding of the spatial spectrum of intensity fluctuations in this regime.

On the positive side, a simple correction of differential indices removes most of the bias in the turbulence integral and seeing. This is illustrated in Fig. 11.

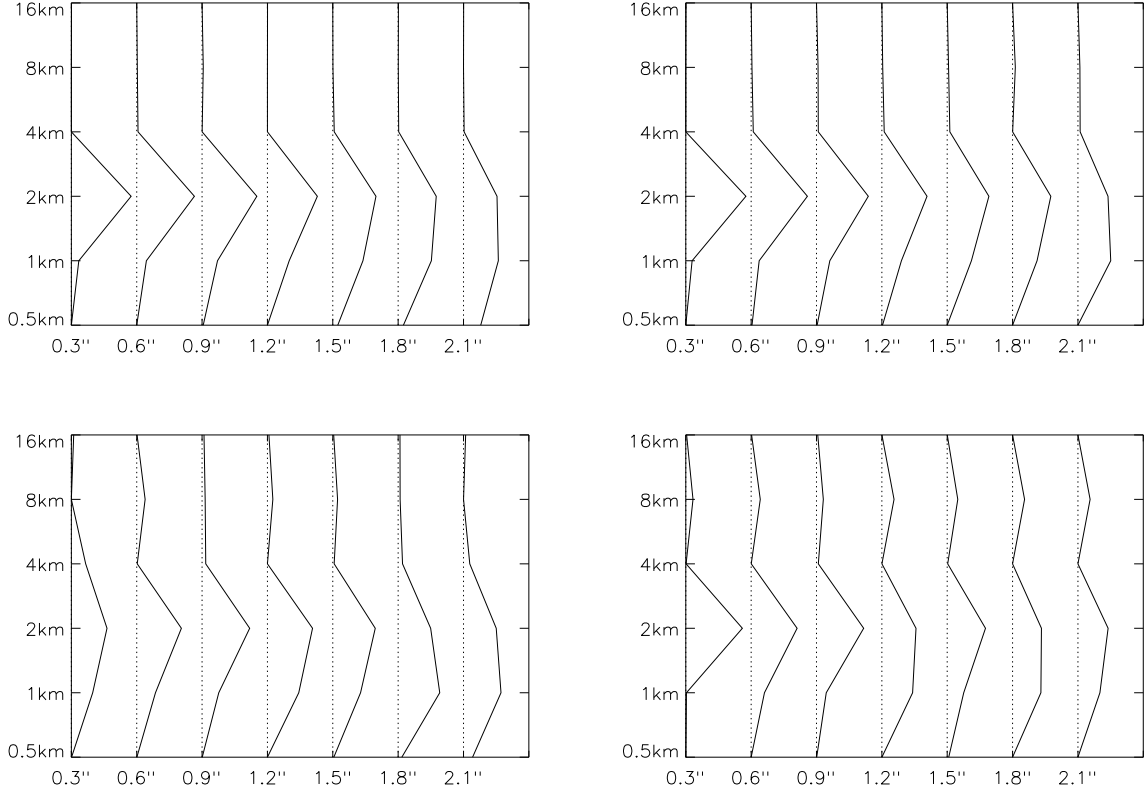


Figure 9: Normalized turbulence profiles restored from the uncorrected indices (left) and corrected indices (right) vs. seeing. The top pair is for profile 1, the bottom pair – for profile 2.

3.5 Exposure-time correction

To be written. It was clear already from the Appl. Opt. (2002) paper that the linear extrapolation over-corrects. The effect is, at worst, 10% on the turbulence integrals (6% on seeing). A simple modification of the correction is sufficient to remove this bias.

4 Conclusions

The current interpretation of the MASS signal in the framework of the weak-scintillation theory is shown to fail even under moderate scintillation. Moreover, the initial guess that the seeing is underestimated turned out to be wrong: under partial saturation the seeing is over-estimated, explaining the “over-shoots” of MASS compared to DIMM.

A deeper insight is required to understand fully the modification of the scintillation spatial spectrum caused by the saturation. Until then, a simple *ad hoc* correction of the measured scintillation indices may be used to remove most of the bias in seeing. This finding is very important for correct comparisons between MASS and DIMM and for estimating the intensity of ground-layer turbulence from their difference.

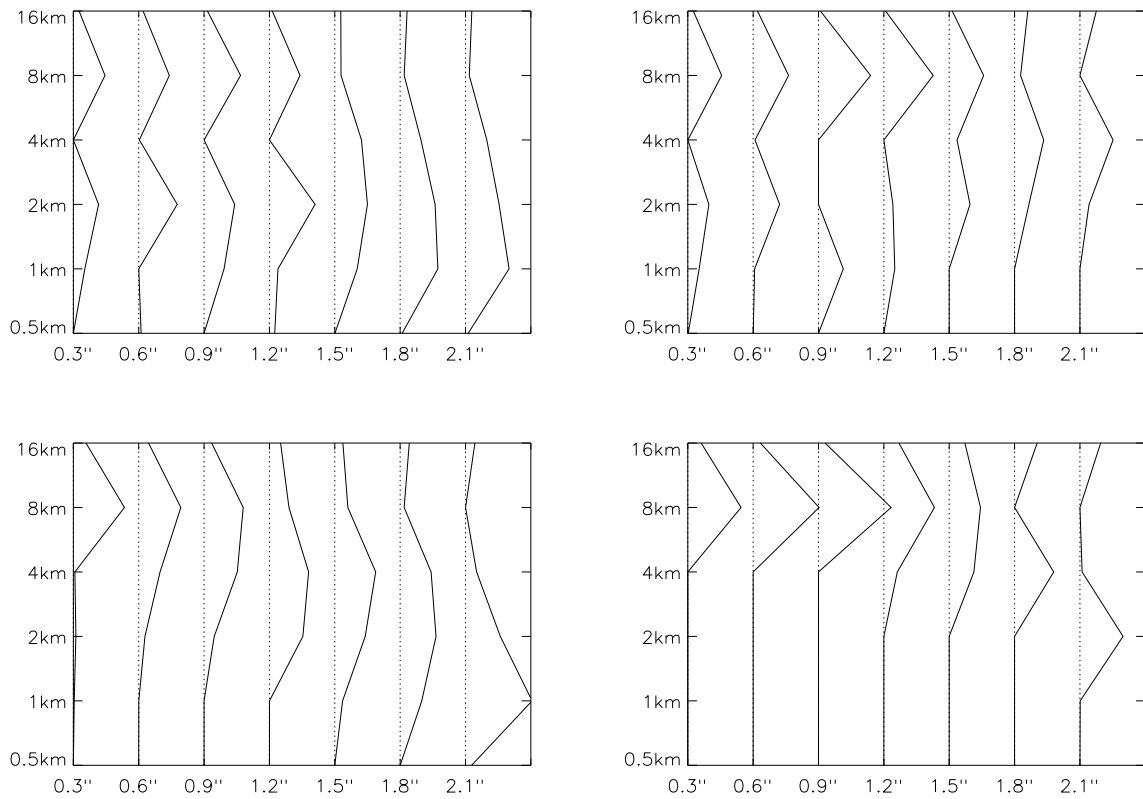


Figure 10: Normalized turbulence profiles restored from the uncorrected indices (left) and corrected indices (right) vs. seeing. The top pair is for profile 3, the bottom pair – for profile 4.

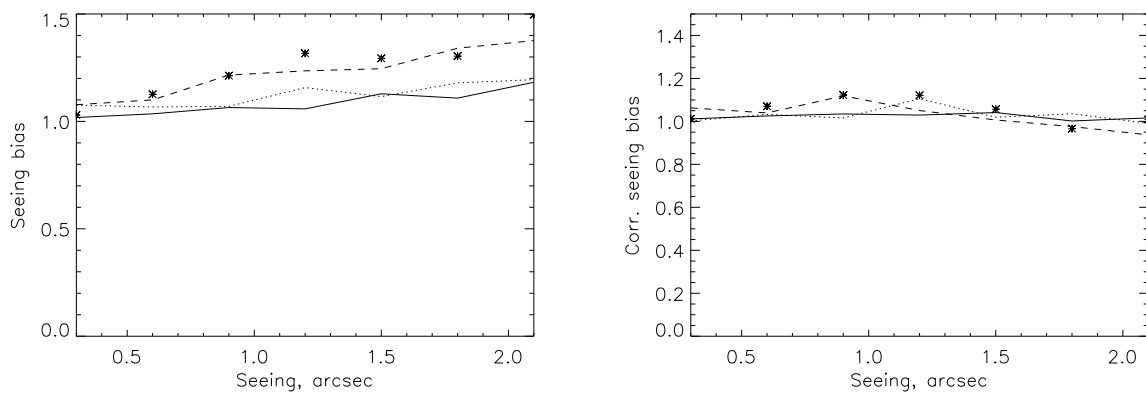


Figure 11: The bias in seeing deduced from the profiles (left – uncorrected indices, right – corrected). All 4 profiles are plotted with the same notation as in Fig. 8.